Physics of the Earth and Planetary Interiors 223 (2013) 8–20

Contents lists available at SciVerse ScienceDirect

Physics of the Earth and Planetary Interiors

journal homepage: www.elsevier.com/locate/pepi

Aspherical structural heterogeneity within the uppermost inner core: Insights into the hemispherical boundaries and core formation

Meghan S. Miller [a,*], Fenglin Niu [b,c], Elizabeth A. Vanacore [d]

[a] University of Southern California, Department of Earth Sciences, Los Angeles, CA, United States
[b] State Key Laboratory of Petroleum Resource and Prospecting, and Unconventional Natural Gas Institute, China University of Petroleum, Beijing, China
[c] Rice University, Department of Earth Science, Houston, TX, United States
[d] University of Leeds, Department of Earth Sciences, Leeds, UK

ARTICLE INFO

Article history:
Available online 7 March 2013
Edited by George Helffrich

Keywords:
Inner core
Attenuation
PKP phases
Differential travel times
Boundary structure

ABSTRACT

Lateral heterogeneities at the top of the inner core are investigated using earthquakes that occurred in Indonesia and southeast Asia and were recorded in the southeastern Caribbean. Using seismic observations of attenuation and seismic velocity, we were able to constrain the characteristics of the boundary between the inner and outer core to further investigate the dynamics and evolution of the Earth's core. Our seismic observations from core phases confirm that the outermost inner core is asymmetrically heterogeneous and we are able to further constrain the morphology and physical properties of this layer. Comparison of data from earthquakes with ray paths traversing from east to the west versus those with ray paths from west to east allow us to map the aspherical heterogeneity of the boundary layer and specifically image the boundary between the proposed quasi-eastern and western hemispheres of the inner core. The variation of differential travel times between PKP_{df} and PKP_{bc}, attenuation in terms of Q factor, and latitudinal changes for both of these observations, can be attributed to localized heterogeneity at the quasi-hemispherical boundaries of the inner core. We constrain the change in the thickness of outermost core boundary layer from 100 to 250 km within a distance of a few 10s of kilometers at 45°E ± 2°, for the western boundary, with an overall P-wave velocity decrease in the western hemisphere of 0.5% and increase of 0.5% in the eastern hemisphere. We constrain the eastern boundary at latitudes greater than 45°N to 173°E ± 4° with an overall P-wave velocity decrease in the western hemisphere of 1.0% in the uppermost 200 km of the inner core. The eastern boundary at equatorial latitudes is constrained to a region <170°E with a western hemisphere with a 0.5% drop in P-wave velocity in the uppermost 250 km.

1. Introduction

Evidence of aspherical structure of the inner core using body wave data began with the investigation of travel times of PKP_{df} (PKIKP) (Poupinet et al., 1983). Much of our knowledge of the inner core is based on the observation of this phase, PKP_{df}, which travels through the solid inner core, and the differential travel times between it and PKP_{bc}, a P wave which travels through the deep portion of the liquid outer core (Fig. 1A). Since these two compressional waves have similar ray paths in the mantle and much of the outer core, the differences in travel times and amplitudes between PKP_{bc} and PKP_{df} can be attributed to the vicinity of the inner core boundary. However, the use of these phases have been challenged for accurately interpreting structure in the inner core (Ishii et al., 2002; Romanowicz et al., 2002). As seismic data sets have dramatically improved due to a more extensive distribution of instruments across the Earth over the last 25 years, there has been advancement in the understanding of the complex structure of the inner core.

From analysis of these enhanced data it has been found that the inner core is not simply just a solid, but has distinct structure and heterogeneity, which can be described in terms of attenuation (Q, quality factor), anisotropy, and seismic velocity. Q, which is a dimensionless quantity, is inversely related to strength of the attenuation, so regions with a high Q are less attenuating and those with a low Q are more attenuating. Unlike the outer core, which has a Q-value that is almost infinite (Dziewonski and Anderson, 1981), the inner core Q-value has been constrained to values less than 450 (Bhattacharyya et al., 1993). The dramatic change in Q occurs at the inner core boundary and appears to happen within the outermost inner core (Song, 1997). Furthermore, it has been suggested that the inner core is separated into two quasi-hemispheres, with boundaries at ~40°E and ~180°W (Tanaka and Hamaguchi, 1997; Niu and Wen, 2001; Garcia, 2002; Wen and Niu, 2002; Cao and Romanowicz, 2004; Stroujkova and Cormier, 2004; Garcia et al., 2006), and these differences are best observed from seismic phases that sample the outermost inner core.

* Corresponding author.
E-mail address: msmiller@usc.edu (M.S. Miller).

0031-9201/$ - see front matter © 2013 Elsevier B.V. All rights reserved.
http://dx.doi.org/10.1016/j.pepi.2013.02.001

Here we further investigate the aspherical heterogeneity of the inner core structure by observing differences in the travel time residuals and quality factor (Q) averages for earthquakes sampling the western hemisphere boundary of the inner core from events occurring in Indonesia recorded at a temporary array in the southeast Caribbean in comparison to earthquakes occurring at the Sunda and Banda arcs which travel in the opposite direction and sample the boundary of the opposite inner core hemisphere. This dataset provides us with a description and understanding of the nature of the boundaries of the inner core hemispheres, and also

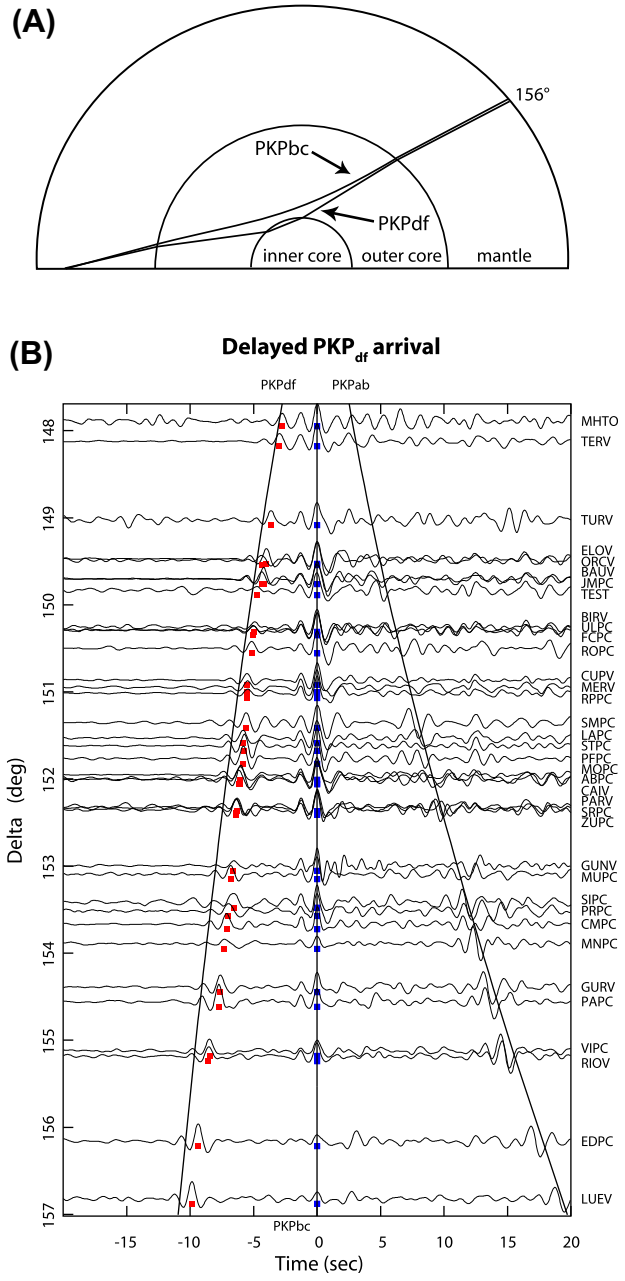

Fig. 1. (A) Ray paths of PKP phases PKP$_{df}$ and PKP$_{bc}$. These two core phases have nearly identical paths through the mantle. (B) Example of a record section for a M_w 5.8 earthquake on 10 April 2002 recorded at the southeastern Caribbean stations. The vertical component seismograms are aligned on PKP$_{bc}$ with station names shown on the right. The red squares are our picks of the PKP$_{df}$ arrival and the blue squares indicate the picked PKP$_{bc}$ arrival. The lines represent the estimated arrival times of the different phases according to PREM (Dziewonski and Anderson, 1981). The horizontal axis (time) is normalized to PKP$_{bc}$. (For interpretation of the references to color in this figure legend, the reader is referred to the web version of this article.)

Table 1
Earthquakes used in inner core boundary study.

Event ID	Latitude	Longitude	Depth (km)	Magnitude (*M*w)
20040107_1845	20.053	122.185	42	5.6
20040410_0735	8.043	137.215	40	5.8
20040701_1928	−5.91	148.662	56	5.6
20040729_0144	12.455	94.997	22	5.9
20040915_1910	14.22	120.411	115	6.0
20041008_1436	13.925	120.534	105	6.5
20041029_1928	15.643	119.11	21	5.5
20041105_0518	−4.361	143.925	125	6.0
20041128_0736	−3.638	135.445	23	6.2
20041210_0942	10.874	141.781	32	5.5
20041211_0155	−4.613	149.779	541	5.5
20041226_0222	8.868	92.467	15	5.7
20041226_0308	13.745	93.009	30	5.9
20041226_0324	4.473	94.068	26	5.8
20041226_1019	13.462	92.738	26	6.3
20041227_0032	5.476	94.467	33	5.8
20041227_0049	12.982	92.395	23	5.8
20041227_0939	5.348	94.65	35	6.1
20041227_1446	12.35	92.469	19	5.6
20041227_1913	11.586	92.499	25	5.5
20041229_0150	9.109	93.756	8	6.1
20041229_1850	5.531	94.277	47	5.7
20041229_2112	5.23	94.625	29	5.6
20041230_1758	12.237	92.515	30	5.7
20041231_1204	6.204	92.913	11	6.0
20050101_0403	5.465	94.398	36	5.7
20050101_0625	5.099	92.304	11	6.6
20050104_1914	10.556	91.727	10	5.7
20050106_0056	5.323	94.835	49	5.7
20050116_2017	10.934	140.842	24	6.6
20050124_0416	7.33	92.482	30	6.3
20050127_0656	7.944	94.059	38	5.7
20050127_2009	5.511	94.306	30	5.5
20050313_2212	5.486	94.595	52	5.5
20050325_0104	5.489	94.374	39	5.9

provides support for the idea that the inner core solidifies from the outer core (Jacobs, 1953), which could be explained by the existence of a mushy zone at the top of the inner core. It has been suggested that as the inner core formed by freezing iron as the liquid outer core gradually cooled, some of the lighter elements in the outer core and may have become concentrated in a mushy or slurry layer at the top of the inner core (Birch, 1964; Gubbins, 1977; Gubbins et al., 2003; Loper, 1978). Using seismic observations of core phases, we are able to constrain the characteristic morphology and properties of the outermost inner core where this layer exists, and from these data learn more about the dynamics and evolution of the Earth.

2. Data

A total of 35 events along the length of the Indonesian archipelago, Papua New Guinea, Mariana arc, and the Philippines recorded by 86 temporary broadband stations in the southeastern Caribbean were used to investigate lateral heterogeneities at the top of the inner core and constrain the physical nature of the boundaries between the eastern and the western quasi-hemispheres (Table 1 and Figs. 1 and 2). Eleven of the events from the Philippines, Papua New Guinea, and the Mariana arc had ray paths that traveled east to the southeastern Caribbean through the core beneath the eastern Pacific and arctic region and the remaining 24 had paths that traveled westward through the core beneath southern Europe and Africa. This dataset contains ray paths that sample the inner core down to 286 km beneath the outer core-inner core boundary providing an excellent dataset to explore this region of the deep Earth. We analyzed events in 2004–2005 with magnitude (M_w)

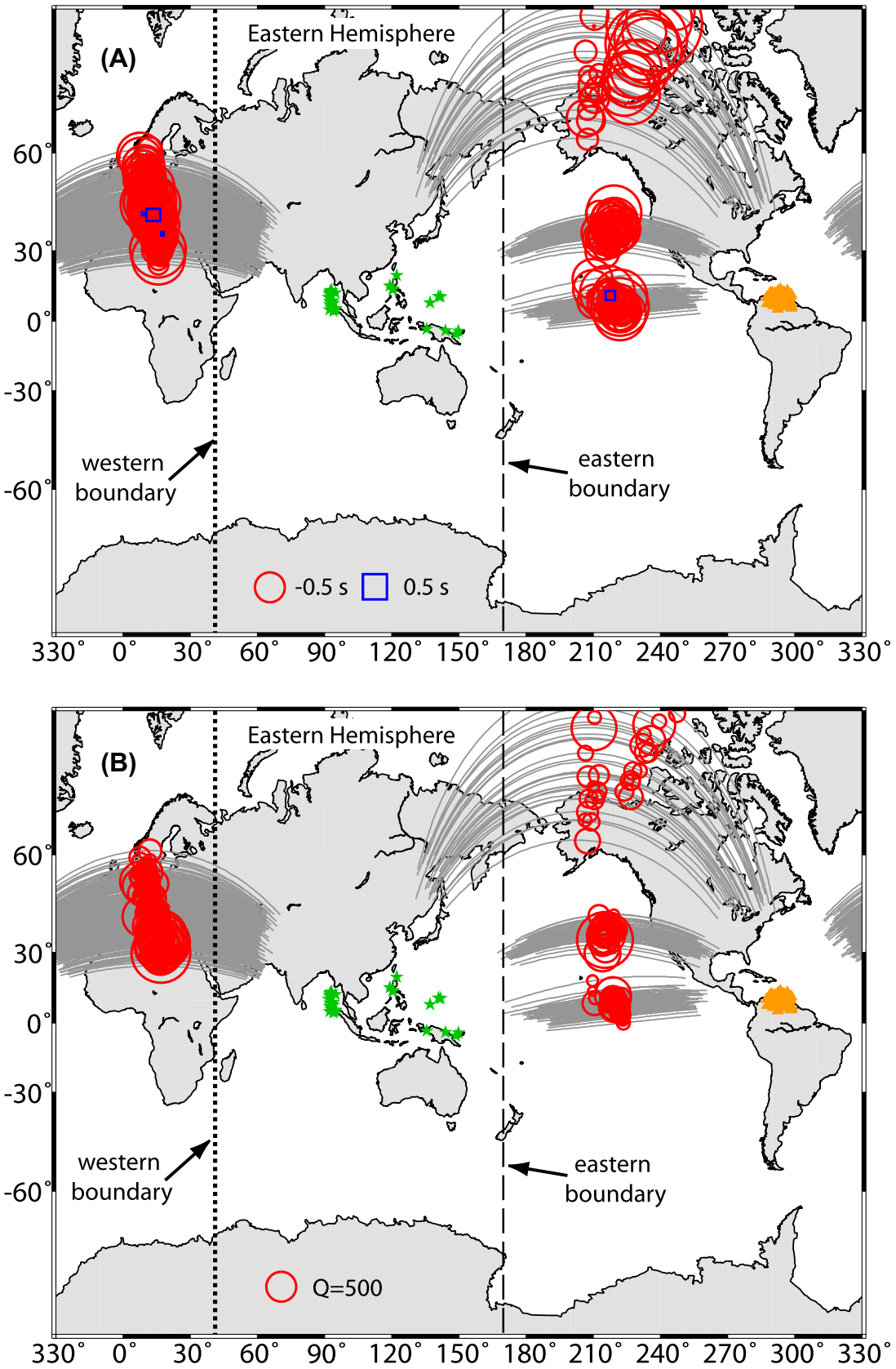

Fig. 2. Map of the turning points of the core phases within the inner core with the ray paths within the inner core plotted in grey. The station locations are plotted as orange triangles and the earthquakes as green stars. The dashed vertical lines indicate the apparent hemispherical boundaries within the inner core. The short, thick dashes mark the western boundary and the long, thin dashes mark the eastern boundary. (A) Red circles represent the delayed arrival of the PKP_{df} phases and blue squares represent the early arrivals, both are scaled by the magnitude of the residuals. (B) Red circles represent the calculated Q values and are scaled according to magnitude. (For interpretation of the references to color in this figure legend, the reader is referred to the web version of this article.)

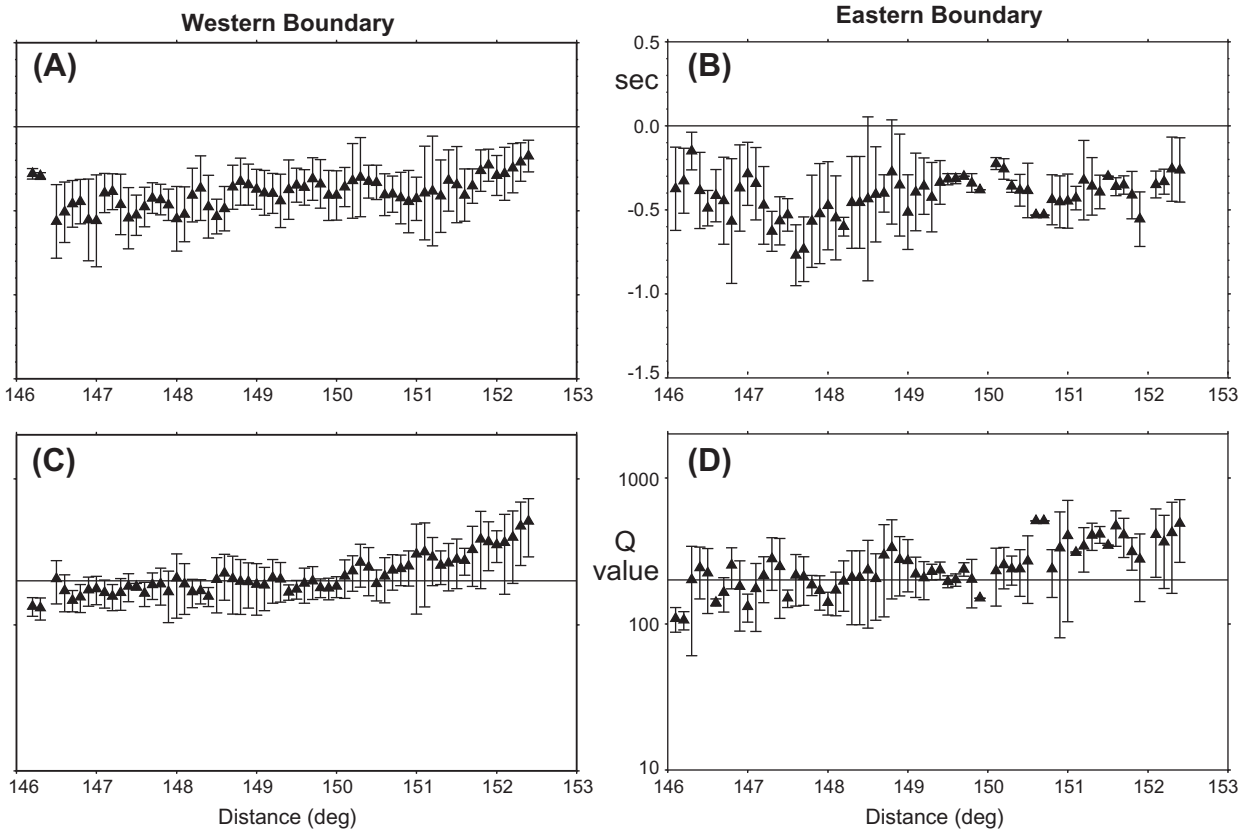

Fig. 3. Plots of the average PKP_{df} arrival time perturbations from the PREM model (Dziewonski and Anderson, 1981) versus distance of the ray path traversed within the inner core (with error bars showing the total range for data within each of the 0.2 degree bins) for events sampling (A) the "western" boundary and (B) the "eastern" boundary of the inner core. (C and D) Plots of the average Q factor values within 0.2 degree bins, with error bars showing the total range for each bin, against distance traversed by the ray path within the inner core for the western and eastern boundaries respectively. Horizontal lines represent a Q factor of 200.

greater than 5.7 and that had a distance range of 135–160° from the PDE catalog. The location of these events resulted in a dense sampling of either the western or eastern boundaries of the inner core in the northern hemisphere.

We first converted the raw broadband velocity records to displacement data by deconvolving the instrument response. We then convolved the displacement data with the WWSSN (WorldWide Standardized Seismograph Network) short-period instrument response as the WWSSN short-period pass band appears to possess the best signal-to-noise ratio (SNR) for the core phases. The data were further filtered with a 2 s low-pass filter and we only selected events that had clear PKP phases with high signal-to-noise ratios (SNR). A typical example of a record section from these events is shown in Fig. 1 with arrivals of PKP_{df} and PKP_{bc} aligned on the peak of the PKP_{bc} arrival. Although PKP_{bc} can be seen up to ~157°, the maximum distance that PKP_{bc} can reach is ~153.07° based on ray theory using the PREM model (Dziewonski and Anderson, 1981) for a 40 km deep source. Beyond this distance the observed PKP_{bc} arrival is the diffracted wave traveling along the ICB due to the finite-frequency nature of seismic waves, therefore its amplitude cannot be approximated by ray theory. The travel time of the diffraction can also be severely affected by 3D structure near the ICB, making the diffracted PKP_{bc} phases not suitable for use as a reference phase. Therefore, in our analysis, we only use PKP_{bc} data up to 152.3°, which is the diffraction distance for a 500 km deep source. We corrected the depths of all the earthquakes to an equivalent depth of 500 km.

To remove the unsuitable diffractions for each earthquake station pair we projected (or corrected) the source depth to 500 km. Then we recalculated the epicentral distances to ensure we do not include unsuitable arrivals in our analyses.

3. Results

3.1. Travel time delays

The differential travel times between PKP_{bc} and PKP_{df} phases are determined by measuring the relative timing between their maximal amplitudes in the WWSSN short-period seismograms. This time picking method has been proven to be very accurate, as the uncertainty in picking the maximal amplitudes is expected to be less than ±0.10 s (Niu and Wen, 2001). We found that almost all of the residuals are negative with respect to PREM (Figs. 3 and 4). There are variations in the magnitude of the negative residuals both with distance (and therefore depth of sampling the inner core) and in longitude and latitude (Figs. 3 and 4). For data sampling the western boundary, the observed residual amplitude seems to decrease with increasing epicentral distance (Fig. 4A), while for those bottoming beneath the eastern boundary, the residual amplitude stays more or less the same over the entire distance range. The negative residuals suggest a negative velocity anomaly at the uppermost inner core with some lateral variability in the anomaly amplitude (Fig. 3). This observation is different than other studies (Kazama et al., 2008; Souriau et al., 2003) which do not sample the boundary of the western hemisphere directly, and observe the opposite trend for distances larger than 150°.

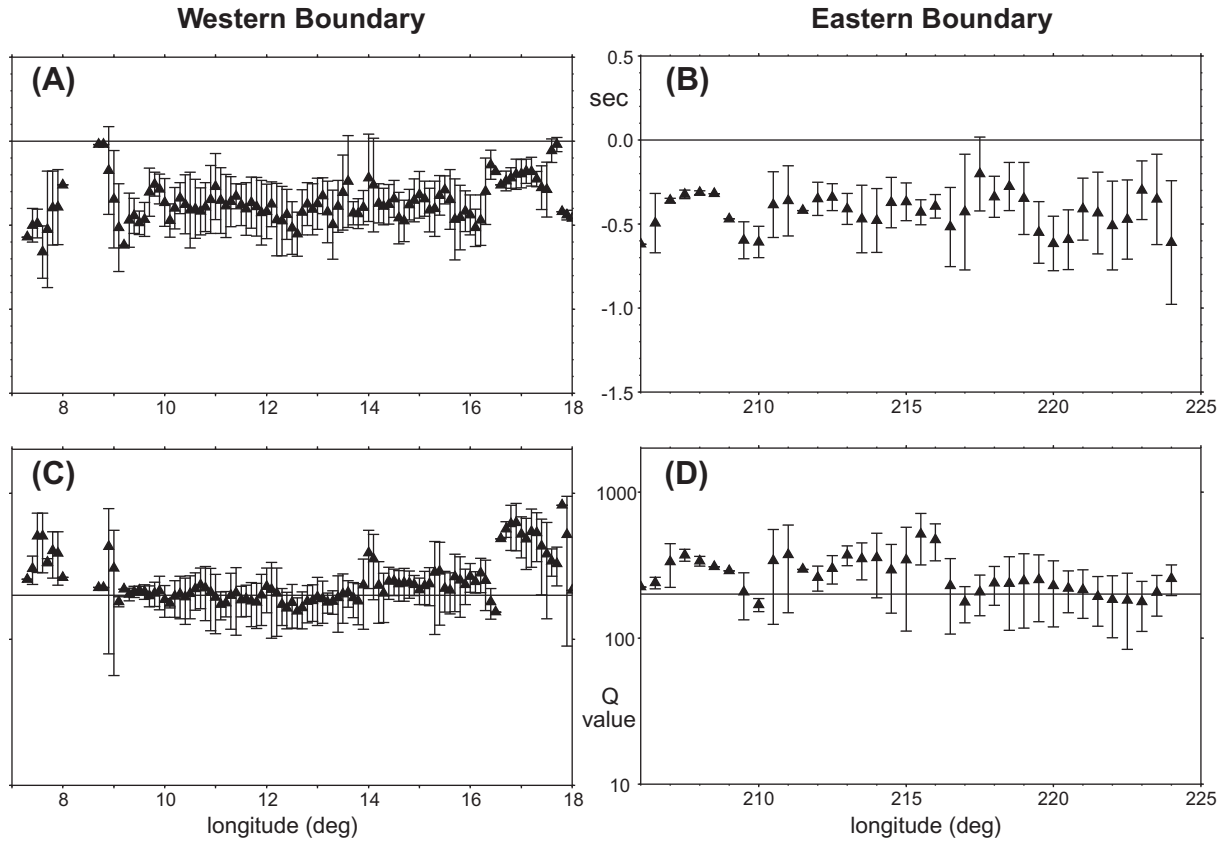

Fig. 4. Plots of average PKP_{df} arrival time perturbations from the PREM model (Dziewonski and Anderson, 1981) versus longitude, with error bars showing the total range for the 0.5 degree bin, of events sampling (A) primarily the "western" hemisphere of the inner core and (B) and partially the "eastern" hemisphere. (C and D) Plots of the average Q within a 0.5 degree bin, with error bars showing the total range for the bin, against longitude for the western and eastern hemisphere, respectively. The horizontal lines represent a Q value of 200.

For the ray paths that traverse from the eastern to the western hemisphere the residuals have an average of −0.4 s and the ray paths that traverse from east to west have residuals with an average of −0.5 s, but the number of observations are slightly smaller (Fig. 3). The range of latitudes sampled at the western boundary is less than that of the eastern boundary, yet it illustrates the localized heterogeneity in the inner core beneath Europe and northern Africa (Fig. 2).

3.2. Attenuation

We first computed the amplitude ratio of PKP_{df}/PKP_{bc} by dividing the maximum amplitudes of the two phases. We then used the observed amplitude ratio to obtain the attenuation structure of the outermost inner core. Since the attenuation of outer core is negligible, the amplitude ratio can be written as:

$$r_{df/bc} = \frac{A_{df}}{A_{bc}} \exp\left\{-\frac{\pi f}{Q} t_{ic}\right\}. \qquad (1)$$
$$Q = -\{\pi f t_{ic}\} \ln r_{df/bc}$$

here A_{df}, A_{bc} and $r_{df/bc}$ are the amplitude of the PKP_{df}, PKP_{bc} and their ratio, respectively. Q is the average quality factor of the inner core, f is the dominant frequency (taken as 1 Hz), and t_{ic} is the travel time of the PKP_{df} ray segment within the inner core. The calculated Q of all the ray paths are shown as a function of epicentral distance and turning point longitude in Figs. 3 and 4, respectively.

At both boundaries, the Q factor shows a gradual increase starting at a distance of ∼151°. We compute synthetic seismograms with the generalized ray theory (Helmberger, 1983) using the PREM model, and found that the amplitude of the PKPbc arrivals starts to decrease at around the same distance due to the diffraction at the ICB. As mentioned above, although the diffraction distance based on ray theory under infinite frequency approximation is around 152.3°, it is expected to occur at closer distance for waves with finite frequency. On the other hand, our synthetics show that the differential traveltime is barely affected by this finite-frequency diffraction.

The average Q factor is approximately 335 ± 50 for the ray paths that sample the eastern boundary but is much lower than those that sample the western hemisphere (∼600 ± 50), as shown in Figs. 3 and 4. This value of Q is a bit lower, but is similar to the western hemisphere values estimated by the study by Cao and Romanowicz (2004) and others (Ivan et al., 2006; Tseng et al., 2001), and higher than the average value (130) that Helffrich et al. (2002) observed. The Cao and Romanowicz (2004) study focuses only on events with distance ranges between 135° and 144°, but we examine events with distance ranges up to 153° due to the nature of the PKP_{df} and PKP_{bc} phases. These authors observe that Q decreases in the western hemisphere as a function of distance, yet we observe that Q increases as a function of distance beyond 146°, although this is greater than the distances they were examining (Fig. 3A and C).

With the two sets of ray paths that sample the eastern and western boundaries we can also investigate the variation in latitude. Latitudinal variations in differential traveltime and Q at the western boundary are shown in Fig. 5A and B. The Q factor is roughly 200 at latitudes between 38°N and 60°N, but significantly increases (∼500) at lower latitudes (25–38°N). The dataset we present samples a similar portion of the inner core compared to the Helffrich

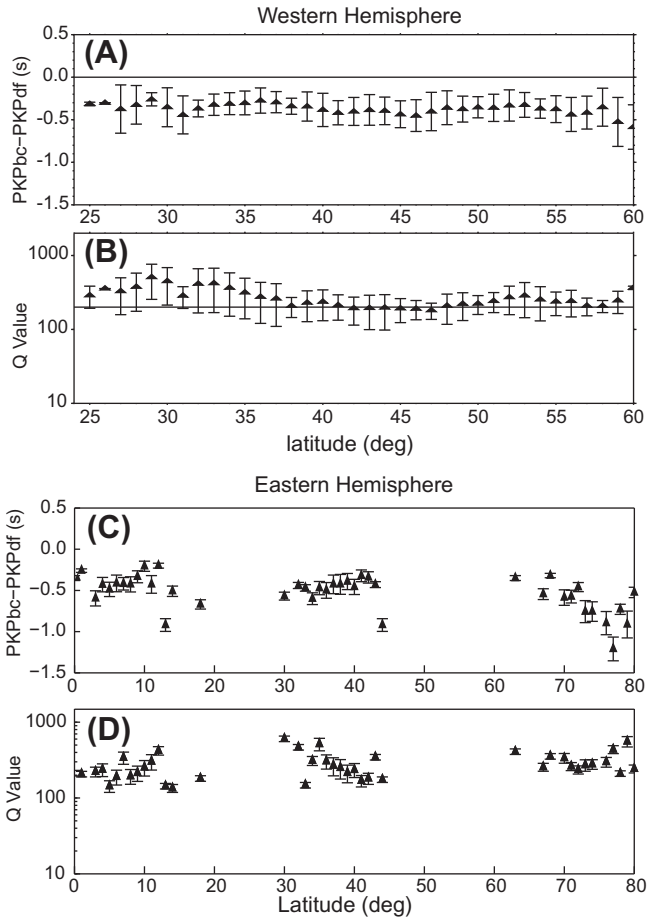

Fig. 5. Plots of (A and C) the averaged time perturbations within one degree bins versus latitude and (B and D) averaged *Q* values versus latitude primarily in the western and eastern hemisphere of the inner core. The error bars show the range of values within each bin.

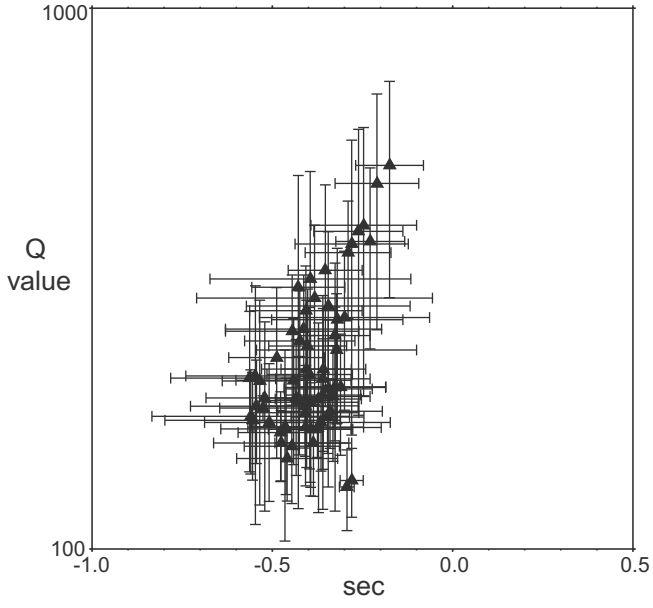

Fig. 6. Averaged Q values (in two degree bins) versus averaged PKP_{df} arrival time perturbations (in 2 degree bins) referenced to the PREM model (Dziewonski and Anderson, 1981) for the western (left) and eastern (right) boundaries.

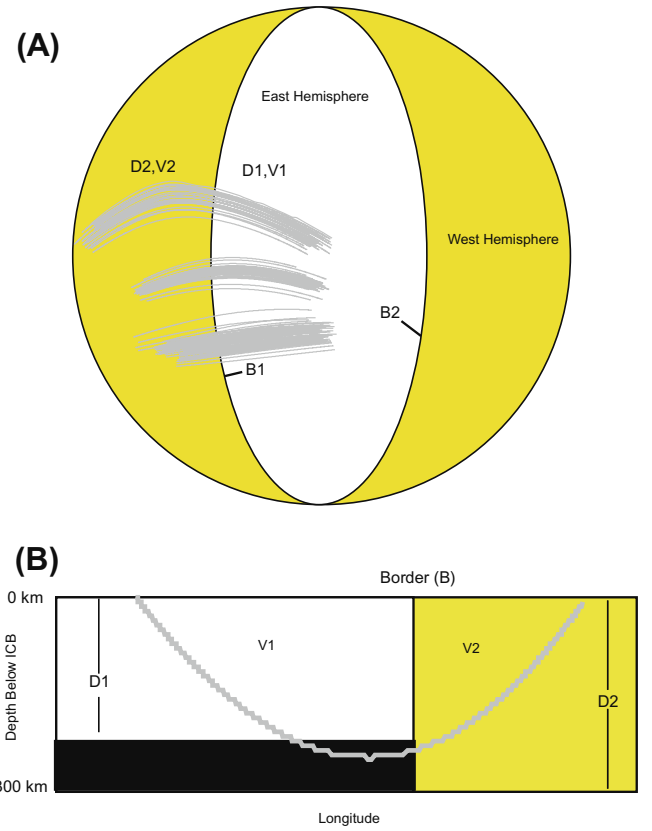

Fig. 7. Schematic drawing of the 2.5D forward modeling scheme where a 2D velocity model is used in combination with 3D ray paths (gray lines). (A) A global map view of the model space with the parameter locations of the eastern hemisphere layer depth, D1, eastern layer velocity, V1, hemisphere boundary location, B1/B2, western layer depth, D2, and western layer velocity, V2, labeled. (B) Cross-section of the 2D model parameterization. The white indicates the zone in the eastern hemisphere perturbed by the D1 and V1 variables. The yellow indicates the region in the western hemisphere perturbed by the D2 and V2 variables. The black indicates the region that is not perturbed from the PREM 1D model. Note that in practice both B1 and B2 are modeled separately, but are referred to as B. (For interpretation of the references to color in this figure legend, the reader is referred to the web version of this article.)

et al. (2002) study, but with opposite direction of ray paths. In the eastern boundary we have fewer sampling points (Fig. 2), but we observe a lower average *Q* factor value (Fig. 5D) than the western boundary.

3.3. Correlations

We found a positive correlation between the residual times and the *Q* factor in the eastern hemisphere beneath northern Africa and Europe (Fig. 6), which is opposite to what has been observed for beneath southern and western Africa (Souriau and Romanowicz, 1996). This positive correlation is, however, similar to other studies that sample the western hemisphere (Kazama et al., 2008; Souriau et al., 2003; Wen and Niu, 2002). Souriau and Romanowicz (1996) focused on differences in *Q* for differing ray azimuths at the inner core turning point in comparison to differential travel times, and they observed that the direction of strong attenuation correlated with that of fast velocity, which is opposite to what we observe for ray paths approximately parallel to the equator. Kazama et al. (2008) observed a positive increase in velocity for events at greater distances than 150°, which they attribute to negative velocity anomaly at the uppermost inner core. Their source-receiver configuration samples a similar portion of the inner core near the west coast of North America (our mid-latitude west to east traversing

rays) using earthquakes from South America recorded in Japan. We do not have the density, nor number of earthquakes they use, but find a similar correlation between the decrease in travel time residuals and distance, which reflects the increase in velocity within the intermediate depth of the inner core.

3.4. Forward modeling

The variation in thickness and structure of the outermost inner core has been identified by other studies, but we have been able to refine the model of morphology and position of the boundary between the hemispheres from these unique event-station pairs. The data in this study encounters the eastern and western border regions at a near perpendicular incidence angle with a limited azimuth range making it ideal for modeling the boundaries. We model the data using a grid search of forward models where free parameters are limited to the border location in longitude (B; also referred to as B1/B2 in Fig. 7), eastern hemisphere layer depth (D1), eastern hemisphere velocity perturbation from PREM (V1), western hemisphere layer depth (D2), and western hemisphere velocity perturbation from PREM (V2). Consequently, the specific geometry of the border is assumed to be an instantaneous step and therefore gradual velocity gradients or more complex geometries are not permitted in the modeling scheme. The forward modeling uses an 2.5D method where the 2D velocity model is projected across all latitudes, but the ray paths travel through the model in a 3D sense (Fig. 7). As usual, we assume a homogenous outer-core and place the travel-time anomaly along the PKP_{df} ray path within the inner core. To calculate the model PKP_{bc}–PKP_{df} travel-time residuals, the method borrows from tomographic techniques whereby we walk along the ray path, determine the node location in the model, and use the model velocity perturbations in slowness and walk step length to calculate the associated travel-time anomaly (e.g. Sambridge and Faletic, 2003). The cumulative travel-time anomaly for each step along the PKP_{df} path through the model is the calculated PKP_{bc}–PKP_{df} travel-time residual. In practice the two sampled borders are modeled and analyzed separately. Furthermore, the eastern boundary is modeled in three separate runs based upon the latitude groupings into the near high latitude (>60°N turning point), mid latitude (25–45°N turning point), an equatorial (<25°N turning point) group to avoid possible contamination due to probable latitudinal variability (Fig. 2).

The uppermost inner core layer depth (D1 and D2) variables are permitted to vary between 50 and 300 km depth below the ICB with 50 km intervals for both the western and eastern hemispheres. This permits modeling down to 300 km beneath the ICB, which is the maximum depth for this study. We limit the velocity space to anomalies (V1 and V2) with ±0%, ±0.5%, ±1% P-wave velocity perturbations from the PREM velocity model. Preliminary models allowing velocity perturbations of up to 1.5% run for the eastern boundary result in significantly larger residual sum-of-squares error (RSS) values that are at a minimum twice as large as the RSS value of acceptable forward models. For each proposed border location in the forward modeling process, we perturb through all possible combinations of D1, V1, D2, and V2 (see Table 2 for range of values). We calculate the residual sum of squares error between the observed and calculated PKP_{bc}–PKP_{df} travel-time residual for each model such that $RSS = \sum(obs - calc)^2$. Forward models with the lowest residual sum of squares error are retained for further analysis.

Most previous studies place the western boundary of the inner core hemispheres between 40°E and 60°E and the eastern boundary between 160°E and 180°E (Tanaka and Hamaguchi, 1997; Creager, 1999; Garcia and Souriau, 2000; Niu and Wen, 2001; Garcia, 2002; Oreshin and Vinnik, 2004; Waszek et al., 2011). One notable exception to this is the recent study of Irving and Duess (2011) that place the western border at 14°E and the eastern border at 151°E. In order to limit the model space to reasonable level and based on our ray path coverage we constrain the border location to 1° intervals between 35–50°E for the western boundary and 160°E–170°W. Additionally, a small-scale test of selected models with a border between 10°E and 20°E for fewer velocity models is conducted to test the viability of the new western border location proposed by Irving and Duess (2011), but testing the 151°E location of the eastern border of the same study is not viable with the data coverage available.

Table 2
Parameter space for each of the variables used in the forward modeling process. For each border location we test all possible combinations of D1-V1 and D2-V2. See Fig. 7 for a graphical view of each variable's meaning.

Variable	Range	Interval
Depth of the eastern hemisphere layer beneath the ICB (D1)	0–300 km	50 km
Depth of the western hemisphere layer beneath the ICB (D2)	0–300 km	50 km
Velocity of the layer in the eastern hemisphere (V1)	−1%*Vp*–1%*Vp*	0.5 %Vp
Velocity of the layer in the western hemisphere (V2)	−1%*Vp*–1%*Vp*	0.5 %Vp
Location of the eastern boundary (B)	160°E–170°W	1°
Location of the western boundary (B)	35–50°E	1°

We use two criteria, RSS and visual inspection of best-fit, to access the final models. Models with large RSS values are immediately eliminated and then only the best 20–30 models in terms of epicentral distance, PKP_{df} turning point, PKP_{df} turning longitude, and PKP_{df} turning latitude are further analyzed. Selected model parameters and resulting RSS values for each of the four geographic modeling sections are summarized in the supplementary data tables in the Appendix (A1). Figs. 8–11 show the preferred models for the western boundary (Fig. 8), the equatorial eastern boundary (Fig. 9), the mid-latitude eastern boundary (Fig. 10), and the high latitude eastern boundary (Fig. 11).

The preferred model of the outermost inner core of the western boundary with a RSS of 10.89 is a boundary at 45°E with a western hemisphere thickness of 250 km and a eastern hemisphere thickness of 150 km (Fig. 8). The velocity of the western hemisphere has a P wave velocity anomaly of −0.5% and the eastern hemisphere has a 0.5% P-wave velocity anomaly. To generate a rough estimate of error on the selected border location for a given velocity model, we hold the velocity model constant to our best-fit case and examine the RSS distribution due to variation of the border location. A plot of the RSS with respect to the border location shows a highly skewed non-Gaussian distribution indicating that estimating the error using typical standard deviations is not appropriate for the data set (Fig. 12). Alternatively, we select an RSS value cutoff using the slope of the RSS curve such that the model range does not encompass the visible strong excursion into high RSS values as the boundary location heads towards 50°E (Fig. 12). A rough estimate of error based upon this process is placed at ±2° where the slope of the RSS model curve reaches ~0.2 RSS/° (Fig. 12A). This value is selected as it demarks where the RSS values and subsequently the absolute value of the curve slope begins to increase dramatically for longitudes heading towards 50°E. Models with the same velocity structure but with a border near 14°E result in a RSS that is double the RSS of our preferred model. The best-fitting model for the hemispherical border near the 14°E proposed by Irving and Duess (2011) with a RSS of 10.97 consists of a boundary location near 18°E with a western hemisphere thickness of 250 km and P-wave velocity drop of 1.0%. The eastern hemisphere has a 0.5% P-wave anomaly in a 100 km thick layer beneath the ICB. Here we prefer the 45°E model for two primary reasons. One, though the RSS value is similar, the

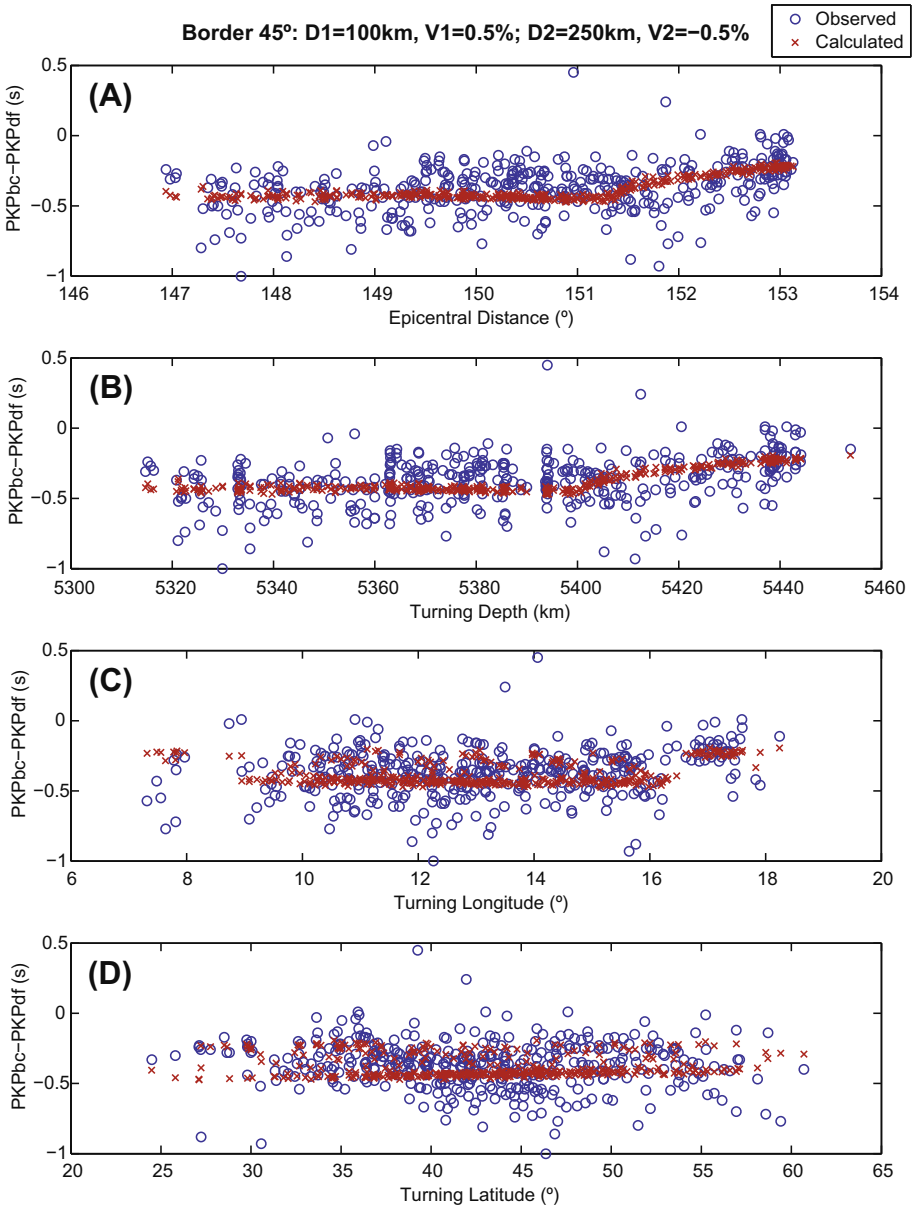

Fig. 8. Results of our preferred model of the outermost inner core at a western boundary at 45° with a western hemisphere thickness of 250 km and a eastern hemisphere thickness of 150 km. The velocity of the western hemisphere has a P wave velocity anomaly of −0.5% and the eastern hemisphere has a 0.5% P-wave velocity anomaly. The observations of the PKP_{bc}–PKP_{df} residuals are shown as blue circles and the red crosses represent the model calculations with respect to epicentral distance (A), PKP_{df} turning depth (B), PKP_{df} turning longitude (C), and PKP_{df} turning latitude. Where D1 or V1 is labeled as XXX and X.X implies there is no layer. (For interpretation of the references to color in this figure legend, the reader is referred to the web version of this article.)

18°E generates a strong structure in the travel time residual plotted with respect to epicentral distance and PKP_{df} turning depth that is not observed in the data (see Fig. A4 in the Appendix). Two, we expect that the modeling is much more sensitive to the structure approximately 200 km below the inner core boundary where the PKP_{df} ray paths turn and have the most lateral resolution. Recent work by Waszek et al. (2011) suggest that this boundary appears to shift eastward with depth below the inner core boundary from ∼10°E for depths of 39–52 km below the ICB to 35–41°E for depths between 69 and 89 km. The 45°E model of this would be consistent with such a migrating boundary given our model sensitivity.

The mid and equatorial latitude data and models do not show evidence of a major excursion in PKP_{bc}–PKP_{df} residuals (Figs. 9 and 10). Additionally, the lowest RSS values are associated models where the ray paths only sample the eastern hemisphere. The most westward inner core entry point of the PKP_{df} ray paths is at ∼170°E; the border location is therefore constrained to a region <170°E. While the boundary location is ill constrained by the data, the velocity structure of the eastern hemisphere can still be modeled. Here our preferred model based on fit to the data is a eastern hemisphere layer at the top of the inner core 200 km thick with a −0.5% P-wave velocity anomaly. In contrast to the low latitude paths, the high latitude data set does appear to sample the eastern boundary (Fig. 11). Our preferred model with a RSS value of ∼2.1 consists of a border location of 173°E ± 4° with a western hemisphere thickness of 250 km and P-wave velocity drop of 1.0%. We find that at this boundary location and western hemisphere velocity structure, the eastern hemisphere velocity cannot be well constrained. Models with no anomalous layer in the eastern hemisphere and models with a 50 km thick layer with P-wave high velocity perturbations of up to 1.0% fit the data

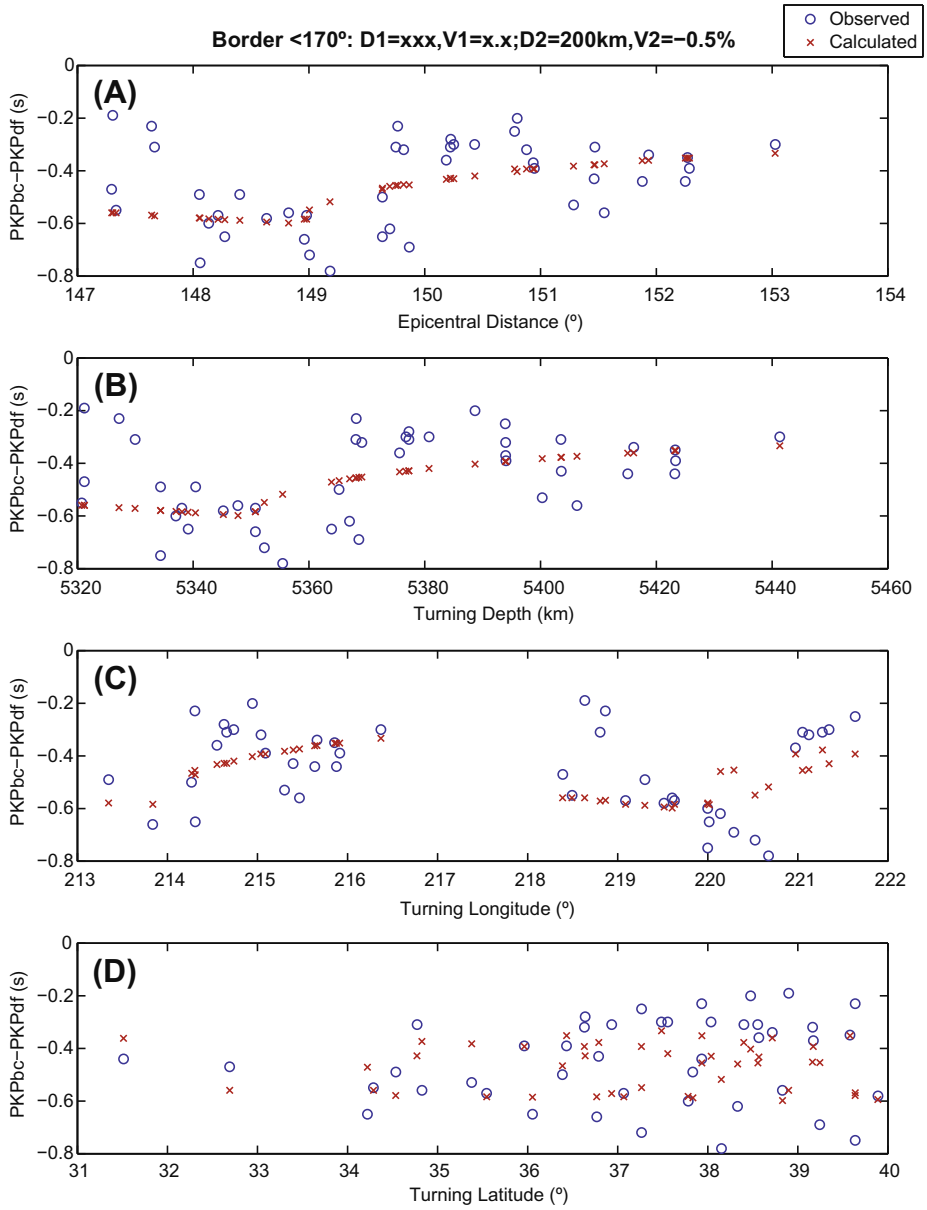

Fig. 9. Same as Fig. 8 but for the mid-latitude (25–45°N) turning point dataset along the eastern boundary. Note that the scaling of the axes has been varied from those used in Fig. 8 to fit this independent dataset.

equally well. The variation between the low latitude and high latitude models indicate that not only is path direction significant in interpreting inner core data but also path location is a factor in modeling the inner core.

4. Discussion

Our seismic observations confirm that the inner core is asymmetrically heterogeneous, specifically the eastern hemisphere has a lower Q-factor and the western hemisphere has a higher Q-factor, which is similar to results from previous studies (Niu and Wen, 2001; Garcia, 2002; Cao and Romanowicz, 2004; Garcia et al., 2006). This is in agreement with the anomalous layer that Stroujkova and Cormier (2004) observed in the equatorial region between 20°W and 140°E, and in a similar observation for the mid-Atlantic that Song and Helmberger (1998) noted from analysis of only one event. Although these studies sample different areas of the eastern hemisphere, it appears that the equatorial anomaly may be a larger feature that we observed beneath eastern Africa (western hemisphere boundary), despite the use of different 1D reference models for some of the studies (Cao and Romanowicz, 2004; Garcia, 2002; Garcia et al., 2006).

With our unique event-station distribution we were able to sample both boundaries and infer the structural morphology of outermost inner core asymmetric quasi-hemispheres (Figs. 2 and 13). Forward modeling of the differential time residuals of the ray paths sampling the western hemisphere boundary indicate that the boundary is located at approximately 45°E, not 40°E as previously suggested (Niu and Wen, 2001), and has a distinct shape. Our forward modeling of the differential time residuals illustrates a possible structure at this hemispherical boundary (Figs. 8–11), which appears to be a "step" type boundary within the outermost inner core at 45°E ± 2°. From the forward modeling and observations of PKP_{bc}–PKP_{df} delay times we suggest that the lower velocity layer of the outermost inner core in the western

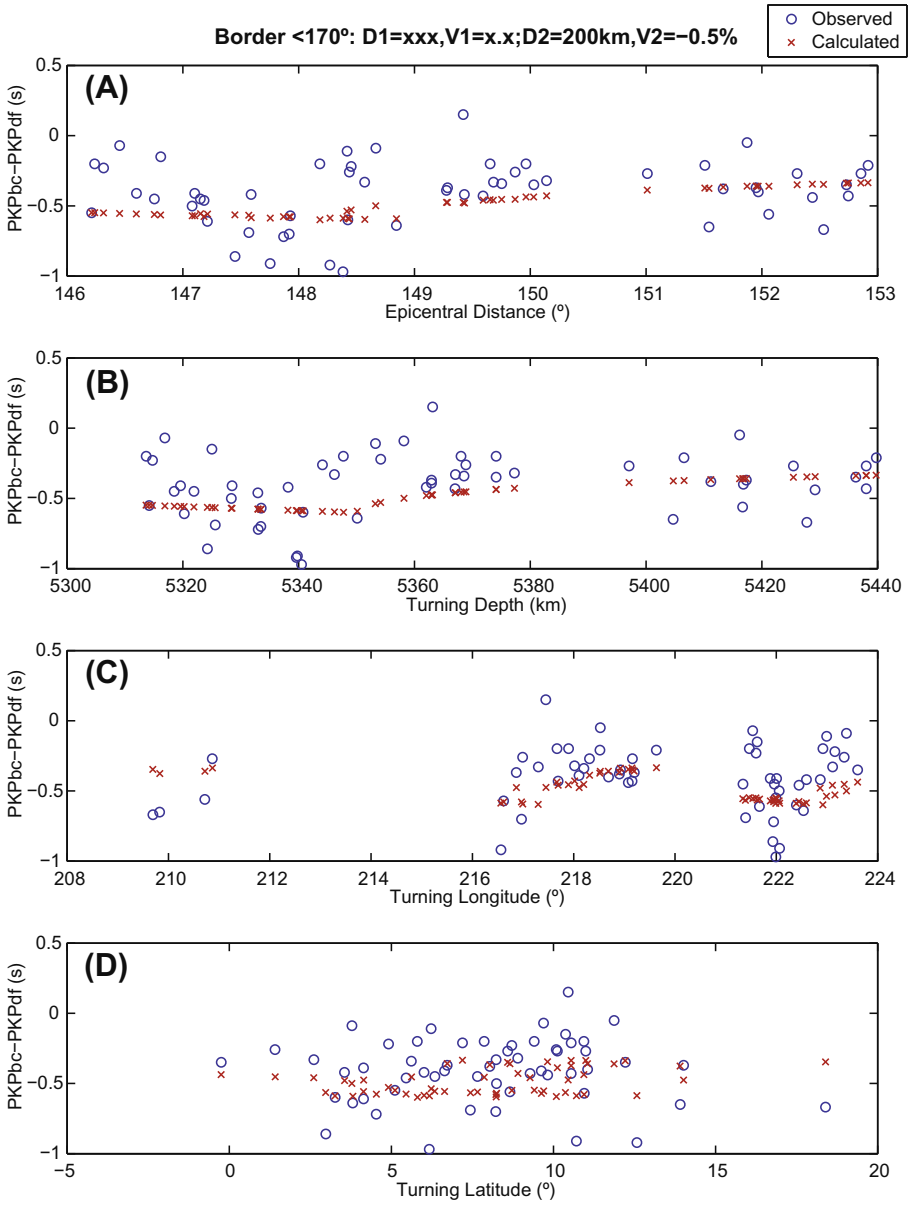

Fig. 10. Same as Fig. 8 but for the equatorial latitude (<25°N) turning point dataset along the eastern boundary. Note that the scaling of the axes has been varied from those used in Fig. 8 to fit this independent dataset.

hemisphere must be thicker than the high velocity layer in the eastern hemisphere. Our best fit model, out of ∼1000 tested, has a western hemisphere layer of 250 km thick and a eastern hemisphere layer that is 150 km thick. We also observe lateral variations in attenuation along the western boundary, in which we infer to not only be a distinct boundary between the hemispheres, but one that varies in latitude.

Our models of PKP_{bc}–PKP_{df} traveltime residuals along the eastern boundary is less constrained when compared to the western boundary models, but the determination of a boundary at 173°E ± 4° at high latitudes and less than ∼170°E at more equatorial latitudes is consistent with previous estimates (e.g. Tanaka and Hamaguchi, 1997; Creager, 1999; Garcia and Souriau, 2000; Niu and Wen, 2001; Garcia, 2002; Oreshin and Vinnik, 2004; Waszek et al., 2011). As with the western boundary modeling we find that the lower velocity western hemisphere requires a thicker layer compared to a thinner or non-existent high velocity layer consequently indicating the existence of a step-like structure between the two quasi-hemispheres. We observe that at different latitudes the data requires different velocity structure in the western hemisphere. The structure appears to transition from a 200 km thick layer with a −0.5% P-wave velocity decrease at equatorial latitudes to a 250 km thick layer with a −1.0% P-wave velocity decrease at high northern latitudes. It has previously been observed by a number of studies that polar paths of PKIKP traveling roughly N–S are anisotropic likely due to alignment of hcp iron (see review by Tromp (2001) for an overview). In this study, however, all the ray paths despite the latitude variation travel quasi perpendicular to the Earth's rotation axis. This indicates that the velocity variation inferred along the eastern boundary is not due to an anisotropic signal but is rather indicative of latitudinal variation along the outermost inner core. Our modeling is based upon ray theory, which of course has its limitations, but modeling of 3D synthetics and numerical simulations is beyond the scope of this study, as are incorporating finite-frequency Fréchet derivatives of body wave travel times (Dahlen et al., 2000). However, Garcia et al. (2006)

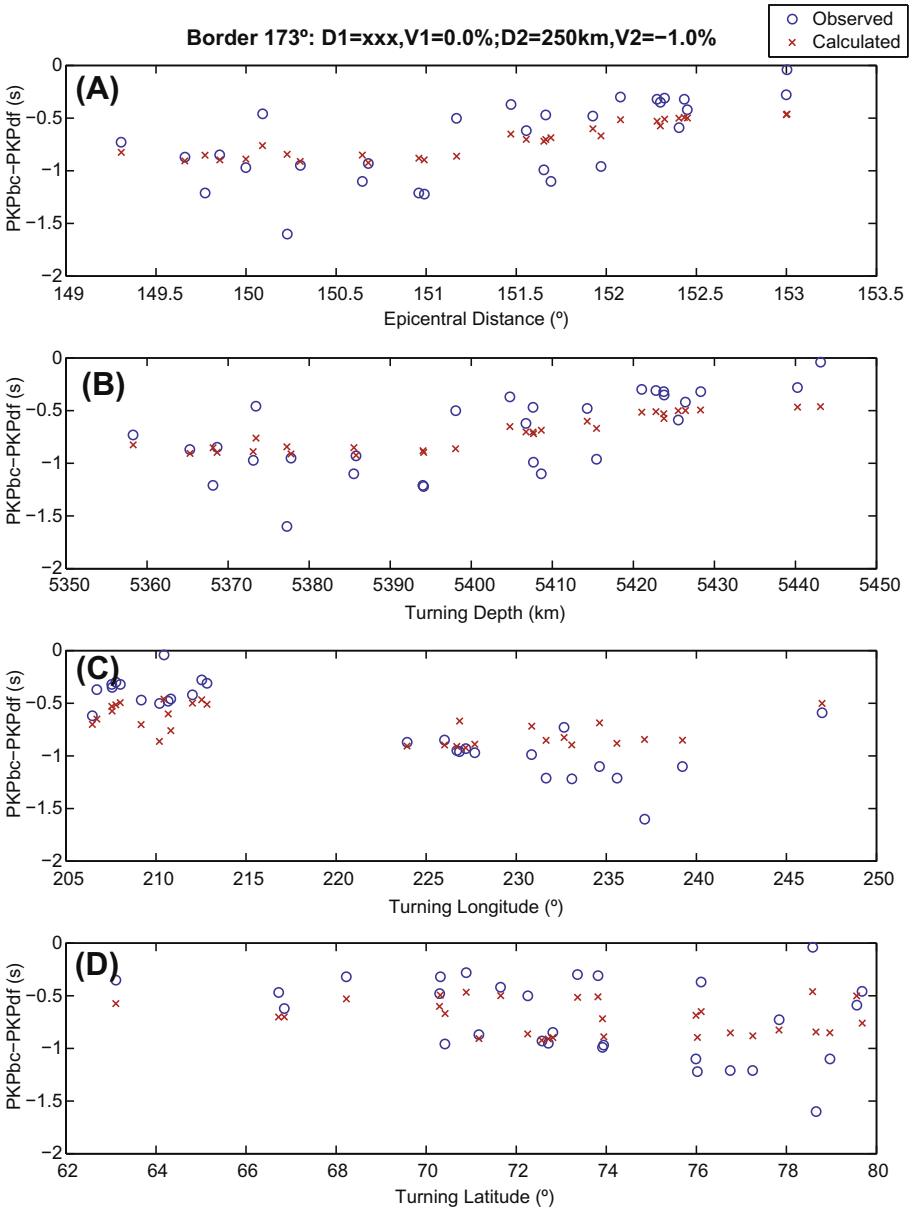

Fig. 11. Same as Fig. 8 but for the equatorial latitude (>45°N) turning point dataset along the eastern boundary. Note that the scaling of the axes has been varied from those used in Fig. 8 to fit this independent dataset.

did use a more sophisticated methodology based on Garcia et al. (2004), where their approach utilizes determining seismological observables to be used in finite-frequency tomography based on 3D sensitivity kernels, and their results generally agree with ours. We also want to point out that our models may not be unique. The ray theory based traveltime analysis essentially has no constraint on the lateral extent of the two boundaries: i.e., whether they are sharp or gradually changing boundaries.

A model that may explain the both the latitudinal Q variations along the hemispherical boundaries in the inner core, as well as the change in residual travel times of PKIKP is not simple. As in previous studies of inner core attenuation, it appears that some, if not most of attenuation may be due to scattering (Cormier, 2007; Koper et al., 2004; Leyton and Koper, 2007; Poupinet and Kennett, 2004; Tkalcic and Kennett, 2008). Koper et al. (2004) and Leyton and Koper (2007) suggest that coda shapes of PKiKP are due to volumetric scattering from the small (1–10 km) length scale heterogeneities in the uppermost inner core. These variations could be due to multiple sources, but are all related to the lateral variations in outer core flow near the inner core boundary and solidification of the inner core from the outer core. Cormier (2007) propose a qualitative model that suggests lateral variations in flow near the inner-core boundary could be the result of texture, which is due to more active solidification and efficient attenuation in the eastern hemisphere and agrees with the model of thermo-chemical wind couple to the mantle and outer core proposed by Aubert et al. (2008). Another model speculates that more vigorous outer core convection in the eastern hemisphere (Gubbins and Gibbons, 2004) could explain the distinct differences in the seismic observations between the two hemispheres. Yet another slightly different model by Monnereau et al. (2010) suggests that growth of the solid inner core implies an eastward drift of material driven by crystallization in the western hemisphere and melting the eastern hemisphere. Furthermore, it is interesting to note that the latitudinal variations along the hemisphere boundary may be related to the effects of a tangent cylinder region as predicted in computer

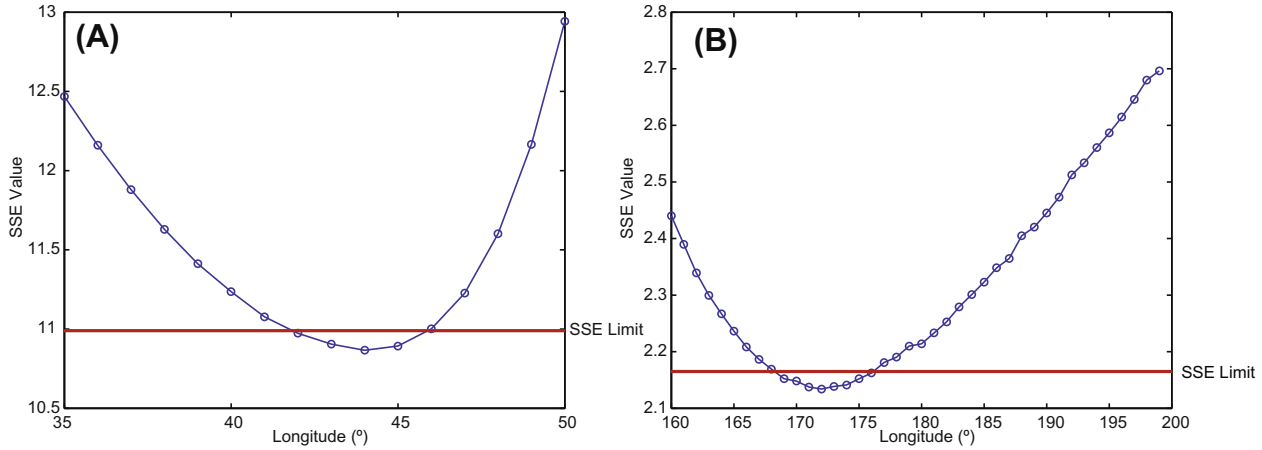

Fig. 12. (a) Graphical representation of the RSS value with respect to border location using our preferred velocity model of the outermost inner core at the western boundary near 45°E described in the text and Fig. 8 caption. The model space has a skewed nature such that statistical estimates of border location error such as standard deviations are not valid. Alternatively, we choose a RSS value limit (red line) below which the absolute value of the slope is less than ~0.2 RSS/°. (b) Same as 12a using the selected velocity model for the eastern boundary near 173°E. In this case due to the significantly lower RSS values, we place the cutoff at a value of ~0.02 RSS/°. (For interpretation of the references to color in this figure legend, the reader is referred to the web version of this article.)

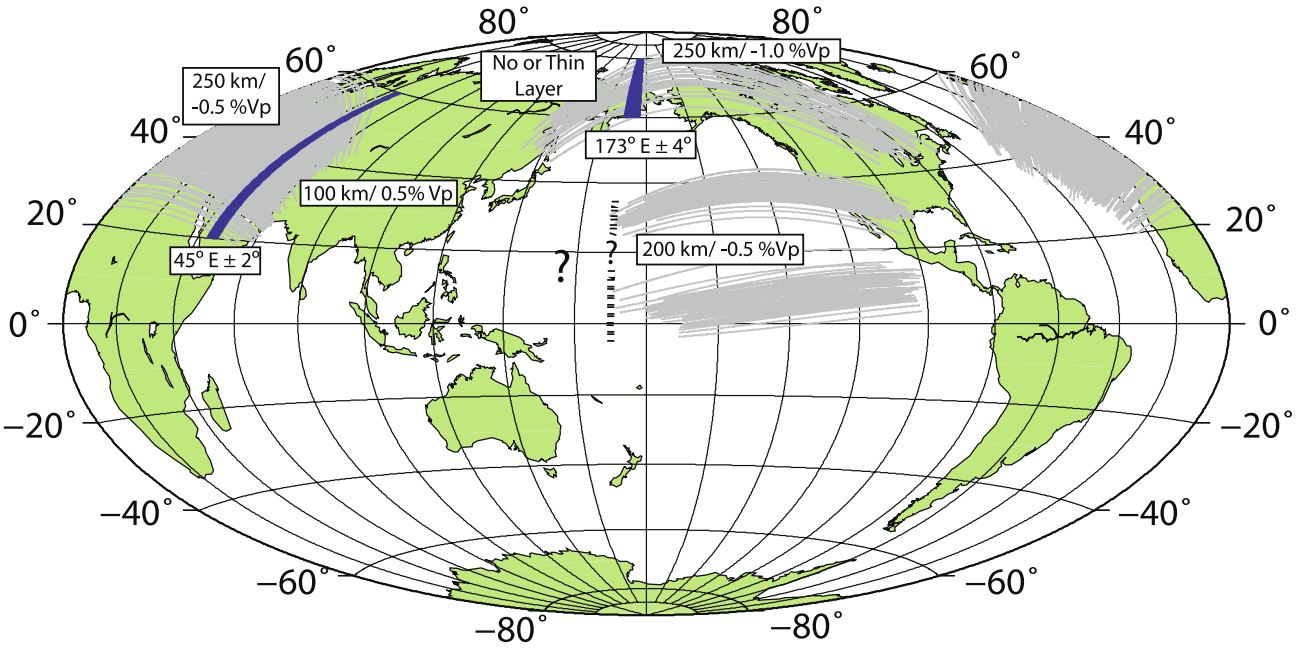

Fig. 13. Geographic representation of the preferred models presented in Figs. 8–11 with the PKP_{df} ray path sampling in the inner core (gray lines). The thick blue lines represent the constrained borders at 45°E ± 2° and 173°E ± 4°; the dotted black line at 170°E represents maximum eastward location of any hemispherical boundary in the outermost inner core based on our dataset. The known velocity perturbations are labeled with the layer thickness and percent change in P-wave velocity relative to the PREM model. (For interpretation of the references to color in this figure legend, the reader is referred to the web version of this article.)

simulations (Glatzmaier and Roberts, 1995). And finally, recent geodynamo simulations suggest that the seismic anomaly observations of variable composition and thickness of the outermost inner core may be the result of heat flux variations (Gubbins et al., 2011). The authors suggest that these regions of flux variations would have areas of melting consisting of exposed, precompressed material and the freezing regions may have layers of unconsolidated mush. As suggested by Aubert et al. (2008), the variations in heat flux could explain seismic anomalies we observe within the inner core but regions of melting would produce even stronger effects and could be very localized.

Therefore, we suggest that the heterogeneity in seismic velocity and attenuation within the outermost inner core is due to differences between convection, heat flux, and solidification and melting rates in each hemisphere, producing different geometric distribution and alignment of iron crystals within the inner core. The boundaries of these two physically distinct regions are now found to be at 45°E and 173°E which is the result of both observations of attenuation and travel time differences of core phases that pass through the quasi-hemisphere boundaries within the outermost inner core.

Acknowledgements

We thank the BOLIVAR team and IRIS for the data. We also thank two reviewers and the editor for very constructive

comments. EV was funded by NERC grant NE/H022473/1 and MSM was funded in part by a NSERC PDF grant. Figures in this paper were generated using the GMT software developed by Wessel and Smith (1990).

Appendix A. Supplementary data

Supplementary data associated with this article can be found, in the online version, at http://dx.doi.org/10.1016/j.pepi.2013.02.001.

References

Aubert, J., Amit, H., Hulot, G., Olson, P., 2008. Thermochemical flows couple the Earth's inner core growth to mantle heterogeneity. Nature 454, 561–758.
Bhattacharyya, J., Shearer, P.M., Masters, G., 1993. Inner core attenuation from sort period PKP(BC) versus PKP(DF) waveforms. Geophysical Journal International 114, 1–11.
Birch, F., 1964. Density and composition of the mantle and core. Journal of Geophysical Research 69, 4377–4388.
Cao, A., Romanowicz, B., 2004. Hemispherical transition of seismic attenuation at the top of the earth's inner core. Earth and Planetary Science Letters 228, 243–253.
Cormier, V.F., 2007. Texture of the uppermost inner core from forward- and back-scattered seismic waves. Earth and Planetary Science Letters 258, 442–453.
Creager, K.C., 1999. Large-scale variations in inner core anisotropy. Journal of Geophysical Research 104, 23127–23139.
Dahlen, F.A., Hungh, S.-H., Nolet, G., 2000. Fréchet kernels for finite-frequency traveltime. I. Theory. Geophysical Journal International 141, 175–203.
Dziewonski, A., Anderson, D.L., 1981. Preliminary reference earth model. Physics of the Earth and Planetary Interiors 25, 297–356.
Garcia, R., 2002. Constraints on upper inner-core structure from waveform inversion of core phases. Geophysical Journal International 150, 651–664.
Garcia, R., Souriau, A., 2000. Inner core anisotropy and heterogeneity level. Geophysical Research Letters 27, 3121–3124.
Garcia, R., Chevrot, S., Weber, M., 2004. Nonlinear waveform and delay time analysis of triplicated core phases. Journal of Geophysical Research 109. http://dx.doi.org/10.1029/2003JB002429.
Garcia, R., Tkalcic, H., Chevrot, S., 2006. A new global PKP data set to study earth's core and deep mantle. Physics of the Earth and Planetary Interiors 159, 15–31.
Glatzmaier, G.A., Roberts, P.H., 1995. A three-dimensional convective dynamo solution with rotating and finitely conducting inner core and mantle. Physics of the Earth and Planetary Interiors 91, 63–75.
Gubbins, D., 1977. Energetics of the earth's core. Journal of Geophysics 43, 453–464.
Gubbins, D., Alfe, D., Masters, G., Price, G.D., Gillan, M.J., 2003. Can the earth's dynamo run on heat alone? Geophysical Journal International 155, 609–622.
Gubbins, D., Gibbons, S.J., 2004. Low pacific secular variation. In: Channell, J.E.T., Kent, D.V., Lowrie, W., Meert, J.G. (Eds.), Timescales of the Internal Geomagnetic Field. AGU, Washington, D.C., pp. 279–286.
Gubbins, D., Sreenivasan, B., Mound, J., Rost, S., 2011. Melting of the earth's inner core. Nature 473, 361–363.
Helffrich, G.R., Kaneshima, K., Kendall, J.-M., 2002. A local, crossing-path study of attenuation and anisotropy of the inner core. Geophysical Research Letters 29. http://dx.doi.org/10.1029/2001GL014059.
Helmberger, D.V., 1983. In earthquakes: observation, theory and interpretation. In: Kanomori, H., (Ed.), Soc. Italiana Di Fisica, Bologna, pp. 173–222.
Irving, J.C.E., Deuss, A., 2011. Hemispherical structure in inner core velocity anisotropy. Journal of Geophysical Research 116, B04307.
Ishii, M., Dziewonski, A.M., Tromp, J., Ekstrom, G., 2002. Joint inversion of normal model and body wave data for inner core anisotropy: 2. Possible complexities:. Journal of Geophysical Research 107. http://dx.doi.org/10.1029/2001JB000713.
Ivan, M., Marza, V., Caixeta, D.d.F., Arraes, T.D.M., 2006. Uppermost inner core attenuation from PKP data observed at some south American seismological stations. Geophysical Journal International 164, 441–448.
Jacobs, J.A., 1953. The earth's inner core. Nature 172, 297–298.
Kazama, T., Kawakatsu, H., Takeuchi, N., 2008. Depth-dependent attenuation structure of the inner core inferred from short-period Hi-net data. Physics of the Earth and Planetary Interiors 167, 155–160.
Koper, K.D., Franks, J.M., Dombrovskaya, M., 2004. Evidence for small-scale heterogeneity in earth's inner core from a global study of PKiKP coda waves. Earth and Planetary Science Letters 228, 227–241.
Leyton, F., Koper, K.D., 2007. Using PKiKP coda to determine inner core structure: 2. Determination of QC. Journal of Geophysical Research 112. http://dx.doi.org/10.1029/2006JB004370.
Loper, D.E., 1978. The gravitationally powered dynamo. Journal of the Royal Astronomical Society 54, 389–404.
Monnereau, M., Calvet, M., Margerin, L., Souriau, A., 2010. Lopsided growth of the earth's inner core. Science 328, 1014–1017.
Niu, F., Wen, L., 2001. Hemispherical variations in seismic velocity at the top of the earth's inner core. Nature 410, 1081–1084.
Oreshin, S., Vinnik, L., 2004. Heterogeneity and anisotropy of seismic attenuation in the inner core. Geophysical Research Letters 31, L02613.
Poupinet, G., Kennett, B.L.N., 2004. On the observation of high frequency PKiKP and its coda in Australia. Physics of the Earth and Planetary Interiors 146, 497–511.
Poupinet, G., Pillet, R., Souriau, A., 1983. Possible heterogeneity of the earth's core deduced from PKIKP travel times. Nature 305, 204–206.
Romanowicz, B., Tkalcic, H., Bréger, L., 2002. On the origin of complexity in PKP travel time data from broadband records. In: Dehant, V., Creager, K.C. (Eds.), Earth's Core: Dynamics, Structure, Rotation, 31. AGU, Washington, D.C., pp. 31–44.
Sambridge, M., Faletic, R., 2003. Adaptive whole Earth tomography. Geochemistry, Geophysics, Geosystems 4, 1022.
Song, X., 1997. Anisotropy of the earth's inner core. Reviews of Geophysics 35, 297–313.
Song, X., Helmberger, D.V., 1998. Seismic evidence for an inner core transition zone. Science 282, 297–924.
Souriau, A., Garcia, R., Poupinet, G., 2003. The seismological picture of the inner core: structure and rotation. C.R. Geosci. 335, 51–63.
Souriau, A., Romanowicz, B., 1996. Anisotropy in inner core attenuation: a new type of data to constrain the nature of the solid core. Geophysical Research Letters 23, 1–4.
Stroujkova, A., Cormier, V.F., 2004. Regional variations in the uppermost 100 km of the earth's inner core. Journal of Geophysical Research, 109. http://dx.doi.org/10.1029/2004JB002976.
Tanaka, S., Hamaguchi, H., 1997. Degree one heterogeneity and hemispherical variation in anisotropy in the inner core from PKP(BC) – PKP(DF) times. Journal of Geophysical Research 102, 2925–2938.
Tkalcic, H., Kennett, B.L.N., 2008. Core structure and heterogeneity: seismological perspective. Australian Journal of Earth Sciences 55, 419–431.
Tromp, J., 2001. Inner core anisotropy and rotation. Annual Review of Earth and Planetary Sciences 29, 47–69.
Tseng, T.L., Huang, B.S., Chin, B.H., 2001. Depth-dependent attenuation in the uppermost inner core from the Taiwan short period seismic array PKP data. Geophysical Research Letters 28, 459–462.
Waszek, L., Irving, J.C.E., Deuss, A., 2011. Reconciling the hemispherical structure of Earth's inner core with its super-rotation. Nature Geoscience 4, 264–267.
Wen, L., Niu, F., 2002. Seismic velocity and attenuation structures in the top of the earth's inner core. Journal of Geophysical Research, 107. http://dx.doi.org/10.1029/2001JB000170.